*J. Biochem.* 2009;146(2)167–172
doi:10.1093/jb/mvp065

# Fast Binding Kinetics and Conserved 3D Structure Underlie the Antagonistic Activity of Mutant TNF: Useful Information for Designing Artificial Proteo-Antagonists

**Yohei Mukai[1,2], Teruya Nakamura[3], Yasuo Yoshioka[2,4], Hiroko Shibata[2], Yasuhiro Abe[2], Tetsuya Nomura[1,2], Madoka Taniai[5], Tsunetaka Ohta[5], Shinsaku Nakagawa[1], Shin-ichi Tsunoda[2], Haruhiko Kamada[2], Yuriko Yamagata[3] and Yasuo Tsutsumi[1,2,*]**

*[1]Graduate School of Pharmaceutical Sciences, Osaka University, 1-6 Yamadaoka, Suita, Osaka 565-0871; [2]Laboratory of Pharmaceutical Proteomics, National Institute of Biomedical Innovation (NiBio), Osaka 567-0085; [3]Graduate School of Pharmaceutical Sciences, Kumamoto University, Kumamoto 862-0973; [4]The Center for Advanced Medical Engineering and Informatics, Osaka University, 1-6 Yamadaoka, Suita, Osaka 565-0871; and [5]Hayashibara Biochemical Laboratories, Inc., 1-2-3 Shimoishii, Okayama 702-8006, Japan*

Received February 18, 2009; accepted March 17, 2009; published online April 22, 2009

**Tumour necrosis factor (TNF) is an important cytokine that induces an inflammatory response predominantly through the TNF receptor-1 (TNFR1). A crucial strategy for the treatment of many autoimmune diseases, therefore, is to block the binding of TNF to TNFR1. We previously identified a TNFR1-selective antagonistic mutant TNF (R1antTNF) from a phage library containing six randomized amino acid residues at the receptor-binding site (amino acids 84–89). Two R1antTNFs, R1antTNF-T2 (A84S, V85T, S86T, Y87H, Q88N and T89Q) and R1antTNF-T8 (A84T, V85P, S86A, Y87I, Q88N and T89R), were successfully isolated from this library. Here, we analysed R1antTNF-T8 using surface plasmon resonance spectroscopy and X-ray crystallography to determine the mechanism underlying the antagonistic activity of R1antTNF. The kinetic association/dissociation parameters of R1antTNF-T8 were higher than those of wild-type TNF, indicating more rapid bond dissociation. X-ray crystallographic analysis suggested that the binding mode of the T89R mutation changed from a hydrophobic to an electrostatic interaction, which may be responsible for the antagonistic behaviour of R1antTNF. Knowledge of these structure–function relationships will facilitate the design of novel TNF inhibitors based on the cytokine structure.**

**Key words: antagonistic activity, mutant, structure–function relationship, tumour necrosis factor (TNF), X-ray crystallography.**

Tumour necrosis factor (TNF) is an important immunity-modulating cytokine that is required for human body's defence against infectious diseases and carcinogenesis (*1*). Excess TNF, however, causes various autoimmune diseases, such as rheumatoid arthritis, Crohn's disease and ulcerative colitis. Anti-TNF antibodies and soluble TNF receptors (TNFR), which interfere with the activity of TNF, are currently used to treat various inflammatory diseases (*2–4*). Unfortunately, however, because these therapies also inhibit the TNF-host defence function of the patients, they can cause serious side effects, such as bacterial and viral infection, lymphoma development and lupus inflammatory disease (*5–7*). TNF-blockade in patients with multiple sclerosis can aggravate their symptoms (*8*). TNF exerts its biologic functions by binding to two receptor subtypes, p55 TNFR (TNFR1) and p75 TNFR (TNFR2) (*9*). Many autoimmune diseases related to TNF are triggered by the activation of TNFR1, therefore selective TNFR1 blockade may be a useful therapeutic strategy (*10*). Towards this aim, we previously isolated a TNFR1-selective antagonistic TNF mutant (R1antTNF) using a phage display system (*11*).

In our previous report, we constructed a phage library that displays structural variants of the human TNF in which random amino acids were exchanged for the six residues (amino acids 84–89) predicted to be in the TNF receptor-binding site based on the crystal structure of the lymphotoxin-α (LT-α)–TNFR1 complex (*12*). To isolate a TNFR1-selective mutant TNF antagonist, the phage library, comprising $1 \times 10^7$ independent clones, was subjected to two rounds of affinity panning against the human TNFR1 (hTNFR1). Although many of the isolated phage clones induced strong cytotoxicity, some phage clones had almost no cytotoxicity but still had a significant affinity for TNFR1. These non-toxic antagonist candidates (10 clones) were assessed further. The bioactivities and antagonistic activities of recombinant candidates expressed in *Escherichia coli* were measured using the highly TNF-sensitive tumorigenic murine fibroblast cells, L–M cells. Clones T2, T6, T7 and T8 did not activate TNFR1, even when tested at high

*To whom correspondence should be addressed.
Tel: +81-6-6879-8230, Fax: +81-6-6879-8234,
E-mail: ytsutsumi@phs.osaka-u.ac.jp

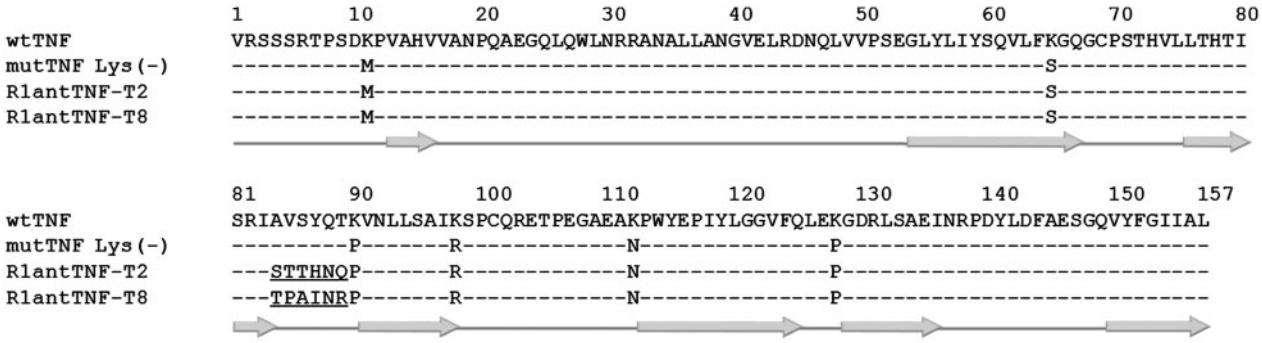


Fig. 1. **Sequence alignment of R1antTNFs and wtTNF.** R1antTNF-T8 and R1antTNF-T2 were created using a phage display system based on a previously reported Lys-deficient TNF mutant (mutTNF Lys(−); K11M, K65S, K90P, K98R, K112N and K128P) (*14*). mutTNF Lys(−) retained full bioactivity and affinity to TNFR. R1antTNFs were mutated in residues 84–89 (underlined), the receptor binding loop. The secondary structure is shown below the TNF sequence (β-sheet; arrow, loop; line).

concentrations, whereas clones T2, T7 and T8 efficiently inhibited wild-type (wt) TNF-induced cytotoxicity. Furthermore, clones T2 and T8 did not bind to TNFR2, suggesting that they were TNFR1-selective antagonists with no bioactivity or affinity for TNFR2. Clones T2 and T8 were renamed R1antTNF-T2 and R1antTNF-T8, respectively, and their sequences are shown in Fig. 1.

As wtTNF converts to an antagonistic TNF by mutation of only six residues, an analysis of the structure–function relationship of R1antTNF will provide important information for the design of artificial TNF inhibitors. Our previous X-ray crystallography and kinetic analysis of the mechanism of antagonism by R1antTNF-T2 suggest that R1antTNF-T2 has higher association/dissociation parameters for TNFR1 binding, despite its similar overall structure to wtTNF (*11*). Based on this finding, we hypothesized that the rapid dissociation of R1antTNF-T2 did not allow for the initiation of an adequate TNFR1 signal.

Here, we show the crystal structure and kinetic properties of another antagonistic TNF, R1antTNF-T8, to support this hypothesis. An understanding of the structure and function of these R1antTNFs, combined with bioinformatics techniques may potentially lead to the design of a functional protein, peptide or peptide mimic that will accelerate the development of novel therapeutic strategies against disease-related proteins, such as TNF.

## MATERIALS AND METHODS

*Expression and Purification of TNFs*—The protocol for the expression and purification of recombinant protein used was the same as that described previously (*13*, *14*). Briefly, TNFs were produced in the *E. coli* BL21 (DE3) strain. The inclusion body of each TNF mutant was washed in Triton X-100 and solubilized in 6 M guanidine–HCl, 0.1 M Tris–HCl, pH 8.0 and 2 mM EDTA. Solubilized protein at 10 mg/ml was reduced with 10 mg/ml dithioerythritol for 4 h at room temperature and refolded by 100-fold dilution in a refolding buffer [100 mM Tris–HCl, 2 mM EDTA, 0.5 M arginine and oxidized glutathione (551 mg/l)]. After dialysis with 20 mM Tris–HCl, pH 7.4, containing 100 mM urea, active trimeric proteins were purified by ion exchange chromatography using Q-Sepharose FF (GE Healthcare Ltd). Size-exclusion chromatography was performed using a Superose 12 column (GE Healthcare Ltd). Endotoxin levels of purified TNF mutants were less than 300 pg/mg.

*Kinetic Analysis Using Surface Plasmon Resonance (SPR)*—The binding kinetics of TNFs was analysed using the BIAcore 3000 SPR system (GE Healthcare Ltd). Human TNFR1-Fc (hTNFR1) and mouse TNFR1-Fc (mTNFR1; ALEXIS Corporation, Switzerland) were immobilized on a CM5 sensor chip, resulting in an increase of 3000–5000 resonance units. During the association phase, TNF mutants or wtTNF diluted in the running buffer (HBS-EP) at 78.4 nM, 26.1 nM or 8.7 nM were individually passed over the immobilized TNFR at a flow rate of 20 μl/min. During the dissociation phase, the HBS-EP buffer was applied to the sensor chip at a flow rate of 20 μl/min. The data were analysed with BIAEVALUATION 3.0 software (GE Healthcare Ltd) using a 1:1 binding model.

*Crystallization*—Purified R1antTNF-T8 was concentrated to 10 mg/ml in 20 mM Tris–HCl pH 7.4. Initial screening using a Hampton Crystal Screen 1-2 and Crystal Screen Lite kit (Hampton Research Corporation, Aliso Viejo, CA) was performed using the vapour-diffusion method with hanging drops at 293 K. Drops consisting of 1 μl protein solution (10 mg/ml) and 1 μl reservoir solution were equilibrated against 250 μl reservoir solution in a 24-well VDX$^{TM}$ Plate (Hampton Research Corp.) Micro crystals were obtained with reservoir solution containing 18% $PEG_{8000}$, 0.2 M calcium acetate hydrate and 0.1 M sodium cacodylate pH 6.5. Reservoir solutions of PEG length and concentration were optimized. The final condition was determined with 1 μl of 10 mg/ml protein solution and 1 μl of reservoir solution containing 15% $PEG_{1500}$, 0.2 M calcium acetate hydrate and 0.1 M sodium cacodylate pH 6.5. Typical dimensions of the crystals used for data collection were $0.6 \times 0.3 \times 0.3$ ($mm^3$).

*Data Collection and Refinement*—X-ray diffraction experiments were performed at BL41XU of the large synchrotron radiation facility, SPring-8, in Harima, Japan. A cryoprotectant solution consisting of 15% $PEG_{1500}$, 0.2 M calcium acetate hydrate, 20% glycerol and 0.1 M

Table 1. **Crystallographic parameters and refinement statistics of the R1-6 crystal.**

| | |
|---|---|
| Data collection | |
| Resolution (Å) | 55.7–2.80 (2.90–2.80) |
| Cell constants (Å)[a] | 49.57,111.33,75.38 |
| Space group | $P2_12_12_1$ |
| Measured reflections | 36,333 |
| Unique reflections | 10,337 (930) |
| Completeness (%) | 92.9 (85.6) |
| $R_{merge}$ (%)[b] | 0.244 (0.530) |
| $I/\sigma$ ($I$) | 36.4 (3.16) |
| Refinement statistics | |
| Resolutions (Å) | 50.0–2.80 |
| Reflections used | 9762 |
| $R_{cryst}$ (%)[c] | 0.269 |
| $R_{free}$ (%)[d] | 0.309 |
| Completeness (%) | 90.4 |
| Atoms | |
| Protein; water | 3312; 7 |
| RMSD from ideal | |
| Bond lengths (Å); bond angles (°) | 0.0124; 1.90 |
| B-factor r.m.s. deviation (Å$^2$) | |
| Main-chain bonds; side-chain | 2.18; 2.58 |
| Main-chain angles; side-chain | 4.01; 4.43 |
| Ramachandran plot statistics | |
| Most favoured regions (%) | 75.8 |
| Additionally allowed regions (%) | 21.4 |
| Generously allowed regions (%) | 2.8 |
| Disallowed regions (%) | 0.0 |

Values in parentheses are those for the outer shell. [a]Cell constants are a, b and c. [b]$R_{merge}$. $\Sigma|I-<I>|/\Sigma<I>$, where $I$ is intensity of the observations. [c]$R_{cryst}$. $\Sigma||F_o|-|F_c||/\Sigma|F_o|$, where $F_o$ and $F_c$ are the observed and calculated structure factors, respectively. [d]$R_{free}$ is calculated as for $R_{cryst}$, but for the test set comprising reflections not used in refinement.

sodium cacodylate pH 6.5 was added to each crystallization drop. The crystals were then mounted in nylon loops (Hampton Research Corp.) and flash-cooled in a nitrogen stream at 95 K. Diffraction data were collected in 1.0° oscillation steps and the crystal diffracted X-rays to a 2.8 Å resolution. The data set was processed and scaled using the program HKL2000 (*15*). The crystals belonged to space group $P2_12_12_1$, with unit-cell parameters $a = 49.6$, $b = 111.3$ and $c = 75.4$Å. Molecular replacement was performed by the Molrep Program in ccp4i (*16*) using a crystal structure of the wtTNF (1TNF) (*17*) as a search model. Cycles of manual rebuilding using the O program (*18*) and refinement using the CNS program (*19*) led to a refined structure. Final model validation was performed using the Procheck Program in ccp4i. Results of the model validation using the Procheck program were as follows: 75.8% residues in the most favoured regions; 21.4% residues in the additional allowed regions; 2.8% residues in the generously allowed regions and 0.0% residues in the disallowed regions. The data collection and refinement statistics are shown in Table 1. The model complexes of TNF–TNFR1 and R1antTNF-T8–TNFR1 were constructed based on the crystal structure of the LT-α–TNFR1 complex (*12*) using the superimposing program in ccp4i.

Table 2. **Kinetic parameters of wtTNF and R1antTNF-T8: affinity to human TNFRI (upper panel) and affinity to mouse TNFRI (lower panel).**

| | wtTNF | R1antTNF-T8 |
|---|---|---|
| Human TNFR1-Fc | | |
| $k_{on}$[a] ($\times 10^4\,M^{-1}\,S^{-1}$) | 4.46 | 85.30 |
| $k_{off}$[b] ($\times 10^{-5}\,S^{-1}$) | 8.17 | 81.90 |
| $K_D$[c] ($\times 10^{-9}\,M$) | 1.76 | 0.96 |
| Mouse TNFR1-Fc | | |
| $K_{on}$[a] ($\times 10^6\,m^{-1}\,S^{-1}$) | 1.30 | 5.61 |
| $k_{off}$[b] ($\times 10^{-6}\,S^{-1}$) | 1.06 | 273.67 |
| $K_D$[c]($\times 10^{-11}\,M$) | 0.08 | 0.48 |

[a]Association rate constant. [b]Dissociation rate constant. [c]Equilibrium dissociation constant ($k_{off}/k_{on}$). Each value was calculated by BIAcore 3000 and BIA evaluation 3.0 software.

## RESULTS

*Kinetic Analysis of R1antTNF-T8 Using SPR*—The kinetic properties of R1antTNF-T8 were compared to those of hTNFR1 and mTNFR1 using the BIAcore 3000 SPR system (Table 2). The dissociation constant ($K_D$) of R1antTNF-T8 binding to hTNFR1 was similar to that of the wtTNF, although R1antTNF-T8 had no bioactivity through activation of TNFR1, as described previously (*11*). The dissociation kinetic constants ($k_{off}$) of R1antTNF-T8 for the human and mouse TNFR1 Fc (hTNFR1: $81.9 \times 10^{-4}\,s^{-1}$, mTNFR1: $273.7 \times 10^{-4}\,s^{-1}$) were clearly higher than those of wtTNF (hTNFR1: $8.17 \times 10^{-4}\,s^{-1}$, mTNFR1: $1.06 \times 10^{-4}\,s^{-1}$). Interestingly, they were also higher than those of R1antTNF-T2 (hTNFR1: $28.7 \times 10^{-4}\,s^{-1}$, mTNFR1: $96.6 \times 10^{-4}\,s^{-1}$) previously described (*11*). The association kinetic constants ($k_{on}$) of R1antTNF for hTNFR1 and mTNFR1 were also higher than those of wtTNF.

*R1antTNF-T8 Structure*—The overall structures of the R1antTNF-T8 (PDB code: 2ZPX) and wtTNF (PDB code: 1TNF) trimers were similar and superimposed with a root mean square deviation (rmsd) of 1.08 Å for 420 Cα atoms (Fig. 2a). The structure of each monomer of R1antTNF-T8 was similar (rmsd 0.43–0.59 for 140 Cα atoms), as is the case for the wtTNF trimer (*17*). This structural property is similar to that of R1antTNF-T2 (Fig. 2b). In addition, the overall structures of R1antTNF-T8 and R1antTNF-T2 are similar with an rmsd of 0.89 Å for 420 Cα atoms, suggesting that the common structure of the two R1antTNFs may be an important feature for their antagonistic TNF activity.

It is believed that TNF signalling is initiated by the formation of a complex with three TNFR on the cell surface. However, R1antTNFs cannot trigger TNF signal-retaining binding affinity to TNFR1 (Table 2) (*11*). This finding supports the idea that the shared structural/kinetic properties between R1antTNF-T8 and R1antTNF-T2 underlie their TNF antagonistic activity.

## DISCUSSION

Kinetic analysis and X-ray crystallography studies of R1antTNF-T8, a TNFR1-selective antagonistic TNF mutant, were performed to determine the mechanism of its antagonistic activity. We previously reported that R1antTNFs have unique properties in that it does not

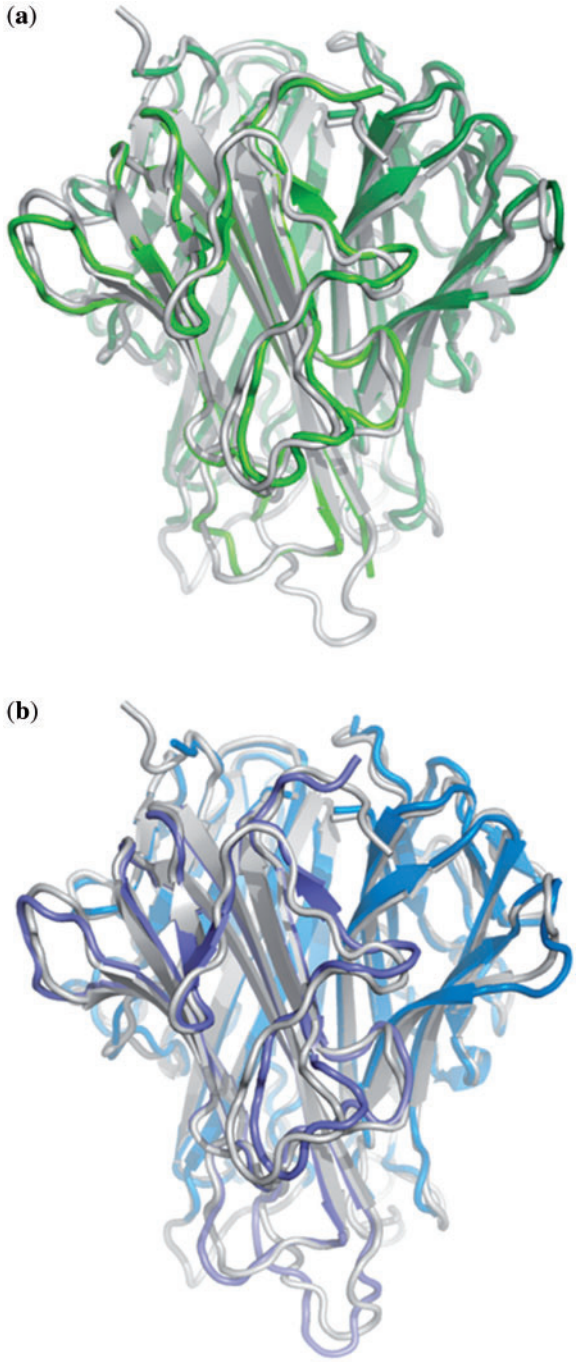


Fig. 2. **Overall structure of wtTNF, R1antTNF-T8 and R1antTNF-T2.** (a) Merged image of previously reported wtTNF structure (grey, 1TNF) and refined R1antTNF-T8 structure (green, 2ZPX). (b) Merged image of wtTNF structure (grey, 1TNF) and R1antTNF-T2 (blue, 2E7A). The flexible loop containing residues 102–110 shown at the bottom of the figure was disordered in the R1antTNF structures. Superimposition of the structures of the wtTNF and R1antTNF was performed using the ccp4i program.

activate TNFR1 despite binding to TNFR1 (*11*). This property allows the mutant TNF to selectively inhibit the TNFR1 signal, which may lead to the design of an effective anti-inflammatory therapy with fewer side effects (*20*). The elucidation of this mechanism will provide useful information for creating novel artificial mutant proteins and inhibitors.

Kinetic analysis of R1antTNF-T8 by SPR indicated that the association and dissociation kinetics are considerably higher than those of wtTNF, indicating that wtTNF and R1antTNF-T8 have different binding patterns. Similar result was also obtained in the case of R1antTNF-T2 (*11*), which suggest that the two R1antTNFs interact with TNFR1 by rapid, repetitive binding and dissociation, and have a binding mode different from that of wtTNF. In addition, the overall structure of R1antTNF-T8 is similar to that of wtTNF and R1antTNF-T2. The structure suggests that R1antTNFs are able to form the TNF–TNFR1 complex for signal initiation without inducing a signal (Fig. 3a) and indicates that R1antTNFs have a different binding mode to TNFR1, an idea supported by their rapid kinetic properties. Because biologically active wtTNF and mutTNF Lys(−) do not show these rapid kinetics, this may be the specific underlying mechanism of the antagonistic activity of R1antTNFs.

To further evaluate the binding pattern, TNF–TNFR1 docking simulation was performed by superimposition. From the model complex of wtTNF–TNFR1, Tyr87 of wtTNF, an essential residue for TNFR1 binding (*21*), was buried in a molecular hydrophobic 'pocket' of TNFR1 in which the receptor residues Leu67 and Leu71 are located (Fig. 3b). Tyr87 in R1antTNF-T8 and R1antTNF-T2 was used to replace other amino acids (Ile87 and His87, respectively; Fig. 3c and d). The structural simulation revealed that Arg89 of R1antTNF-T8 and His87 of R1antTNF-T2 interacted with the relatively negatively charged Ser63 and Asn65 on the TNFR1 surface, which may account for the difference in the association mode compared to wtTNF (Fig. 3c and d). The change from a hydrophobic interaction (Y87) to an electrostatic interaction (Y87H and Y87I/T89R) could cause the unstable, rapid TNFR1 binding pattern that is common to both R1antTNFs.

Furthermore, it is also interesting that the position of a key mutational residue is different in each R1antTNF (Arg89 of R1antTNF-T8 and His87 of R1antTNF-T2). It is thought that we successfully isolated these different R1antTNFs because we used the combinatorial phage library of six randomized amino acids (residues 84–89). From this result, we can also reconfirm that phage display is a powerful tool for isolating mutant proteins that are difficult to design using traditional point mutation methods (*11*, *14*, *22*).

The fact that the rapid binding pattern of these TNF mutants influenced their signal transduction function will be useful for designing artificial drugs and developing more precise tools for basic research. This report also suggested that the fusion of bioinformatics and kinetic/structural analyses would enhance the development of various therapeutic molecules.

## FUNDING

Research for Promoting Technological Seeds (No. 11-067) from the Japan Science and Technology Agency (J.S.T.);

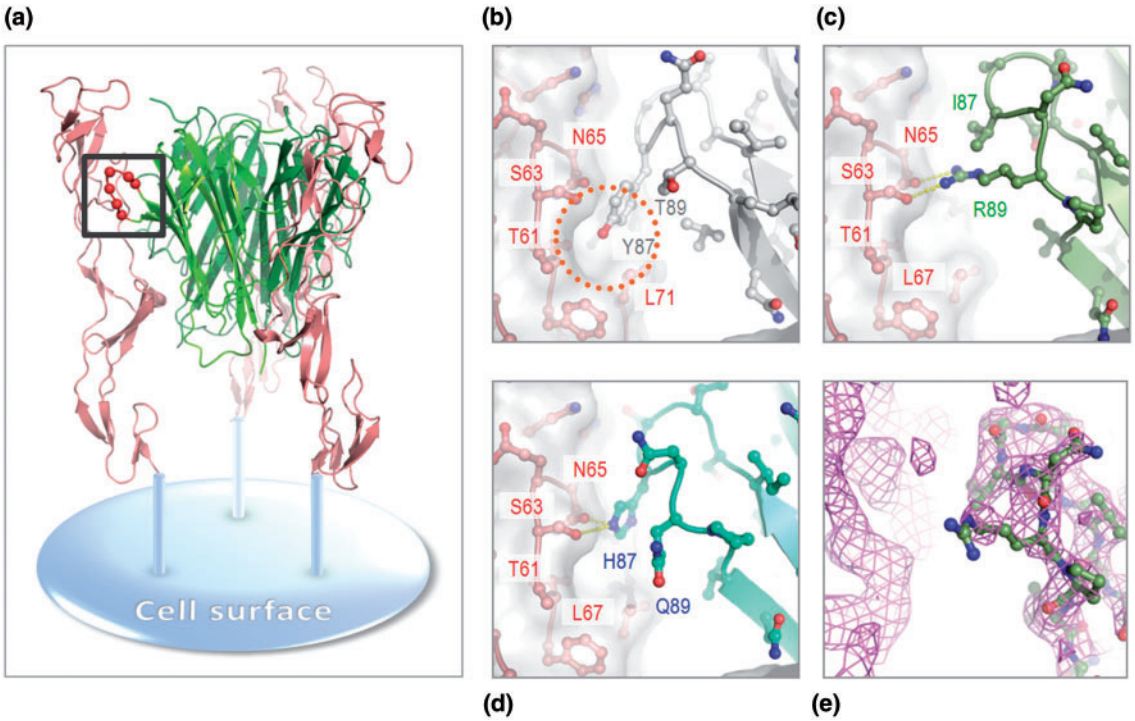


Fig. 3. **Predicted binding model of R1antTNF and TNFR1.** (a) Model complex of R1antTNF-T8 (2ZPX; green cartoon) and TNFR1 (red cartoon) on the cell surface. This complex was built with the Superpose application of the ccp4i program using the LT-α–TNFR1 complex (1TNR). Receptor-binding interfaces corresponding to Fig. 3b–e are indicated by the black square. Mutated residues (amino acids at positions 84–89) are shown as red spheres. (b–d) Receptor-binding interfaces of (b) wtTNF–TNFR1 (grey–red), (c) R1antTNF-T8–TNFR1 (green–red) and (d) R1antTNF-T2–TNFR1 (blue–red). These models were also built with the Superpose application (wtTNF; 1TNF, R1antTNF-T8; 2ZPX, R1antTNF-T2; 2E7A). Critical hydrophobic interaction of wtTNF Y87 and TNFR1 is indicated by the orange circle. In this simulation, the side chains of each structure were rotated to fit the predicted interaction. Stable structures of these rotamers were constructed using the O program. Potential interactions are indicated by yellow dashed lines. (e) 2Fo-Fc map contoured at 0.9 $\sigma$ of R1antTNF-T8 loop (pink mesh).

Research Fund Project on Health Sciences focusing on Drug Innovation (No. KAA3701) from the Japan Health Sciences Foundation; Grants from the Ministry of Health, Labor and Welfare in Japan; Grant-in-Aid for Young Scientists (B) (No. 20790134) and Grants-in-Aid for Scientific Research (Nos. 17016084, 17689008, 17790135, 18015055, 18659047, 20015052 and 20200017) from the Ministry of Education, Culture, Sports, Science and Technology of Japan (MEXT); Research Fellowships for Young Scientists (No. 20-3919) from Japan Society for the Promotion of Science (JSPS).

## CONFLICT OF INTEREST

None declared.

## REFERENCES

1. Aggarwal, B.B. (2003) Signalling pathways of the TNF superfamily: a double-edged sword. *Nat. Rev. Immunol.* **3**, 745–756
2. Feldmann, M. and Maini, R.N. (2003) Lasker Clinical Medical Research Award. TNF defined as a therapeutic target for rheumatoid arthritis and other autoimmune diseases. *Nat. Med.* **9**, 1245–1250
3. Rutgeerts, P., Van Assche, G., and Vermeire, S. (2004) Optimizing anti-TNF treatment in inflammatory bowel disease. *Gastroenterology* **126**, 1593–1610
4. Kooloos, W.M., de Jong, D.J., Huizinga, T.W., and Guchelaar, H.J. (2007) Potential role of pharmacogenetics in anti-TNF treatment of rheumatoid arthritis and Crohn's disease. *Drug Discov. Today* **12**, 125–131
5. Keane, J., Gershon, S., Wise, R.P., Mirabile-Levens, E., Kasznica, J., Schwieterman, W.D., Siegel, J.N., and Braun, M.M. (2001) Tuberculosis associated with infliximab, a tumor necrosis factor alpha-neutralizing agent. *N. Engl. J. Med.* **345**, 1098–1104
6. Shakoor, N., Michalska, M., Harris, C.A., and Block, J.A. (2002) Drug-induced systemic lupus erythematosus associated with etanercept therapy. *Lancet* **359**, 579–580
7. Nathan, D.M., Angus, P.W., and Gibson, P.R. (2006) Hepatitis B and C virus infections and anti-tumor necrosis factor-alpha therapy: guidelines for clinical approach. *J. Gastroenterol. Hepatol.* **21**, 1366–1371
8. Sicotte, N.L. and Voskuhl, R.R. (2001) Onset of multiple sclerosis associated with anti-TNF therapy. *Neurology* **57**, 1885–1888
9. Aggarwal, B.B., Eessalu, T.E., and Hass, P.E. (1985) Characterization of receptors for human tumour necrosis factor and their regulation by gamma-interferon. *Nature* **318**, 665–667
10. Kollias, G. and Kontoyiannis, D. (2002) Role of TNF/TNFR in autoimmunity: specific TNF receptor blockade may be advantageous to anti-TNF treatments. *Cytokine Growth Factor Rev.* **13**, 315–321

11. Shibata, H., Yoshioka, Y., Ohkawa, A., Minowa, K., Mukai, Y., Abe, Y., Taniai, M., Nomura, T., Kayamuro, H., Nabeshi, H., Sugita, T., Imai, S., Nagano, K., Yoshikawa, T., Fujita, T., Nakagawa, S., Yamamoto, A., Ohta, T., Hayakawa, T., Mayumi, T., Vandenabeele, P., Aggarwal, B.B., Nakamura, T., Yamagata, Y., Tsunoda, S., Kamada, H., and Tsutsumi, Y. (2008) Creation and X-ray structure analysis of the tumor necrosis factor receptor-1-selective mutant of a tumor necrosis factor-alpha antagonist. *J. Biol. Chem.* **283**, 998–1007
12. Banner, D.W., D'Arcy, A., Janes, W., Gentz, R., Schoenfeld, H.J., Broger, C., Loetscher, H., and Lesslauer, W. (1993) Crystal structure of the soluble human 55 kd TNF receptor-human TNF beta complex: implications for TNF receptor activation. *Cell* **73**, 431–445
13. Mukai, Y., Shibata, H., Nakamura, T., Yoshioka, Y., Abe, Y., Nomura, T., Taniai, M., Ohta, T., Ikemizu, S., Nakagawa, S., Tsunoda, S., Kamada, H., Yamagata, Y., and Tsutsumi, Y. (2009) Structure–function relationship of tumor necrosis factor (TNF) and its receptor interaction based on 3D structural analysis of a fully active TNFR1-selective TNF mutant. *J. Mol. Biol.* **385**, 1221–1229
14. Yamamoto, Y., Tsutsumi, Y., Yoshioka, Y., Nishibata, T., Kobayashi, K., Okamoto, T., Mukai, Y., Shimizu, T., Nakagawa, S., Nagata, S., and Mayumi, T. (2003) Site-specific PEGylation of a lysine-deficient TNF-alpha with full bioactivity. *Nat. Biotechnol.* **21**, 546–552
15. Otwinowski, Z. and Minor, W. (1997) Processing of X-ray diffraction data collected in oscillation mode. *Methods Enzymol.* **276**, 307–326
16. Potterton, E., Briggs, P., Turkenburg, M., and Dodson, E. (2003) A graphical user interface to the CCP4 program suite. *Acta Crystallogr. D Biol. Crystallogr.* **59**, 1131–1137
17. Eck, M.J. and Sprang, S.R. (1989) The structure of tumor necrosis factor-alpha at 2.6 A resolution. Implications for receptor binding. *J. Biol. Chem.* **264**, 17595–17605
18. Jones, T.A., Zou, J.Y., Cowan, S.W., and Kjeldgaard, M. (1991) Improved methods for building protein models in electron density maps and the location of errors in these models. *Acta Crystallogr. A* **47**, 110–119
19. Brunger, A.T., Adams, P.D., Clore, G.M., DeLano, W.L., Gros, P., Grosse-Kunstleve, R.W., Jiang, J.S., Kuszewski, J., Nilges, M., Pannu, N.S., Read, R.J., Rice, L.M., Simonson, T., and Warren, G.L. (1998) Crystallography & NMR system: a new software suite for macromolecular structure determination. *Acta Crystallogr. D Biol. Crystallogr.* **54**, 905–921
20. Shibata, H., Yoshioka, Y., Ohkawa, A., Abe, Y., Nomura, T., Mukai, Y., Nakagawa, S., Taniai, M., Ohta, T., Mayumi, T., Kamada, H., Tsunoda, S., and Tsutsumi, Y. (2008) The therapeutic effect of TNFR1-selective antagonistic mutant TNF-α in murine hepatitis models. *Cytokine* **44**, 229–233
21. Zhang, X.M., Weber, I., and Chen, M.J. (1992) Site-directed mutational analysis of human tumor necrosis factor-alpha receptor binding site and structure–functional relationship. *J. Biol. Chem.* **267**, 24069–24075
22. Shibata, H., Yoshioka, Y., Ikemizu, S., Kobayashi, K., Yamamoto, Y., Mukai, Y., Okamoto, T., Taniai, M., Kawamura, M., Abe, Y., Nakagawa, S., Hayakawa, T., Nagata, S., Yamagata, Y., Mayumi, T., Kamada, H., and Tsutsumi, Y. (2004) Functionalization of tumor necrosis factor-alpha using phage display technique and PEGylation improves its antitumor therapeutic window. *Clin. Cancer Res.* **10**, 8293–8300